Chapter 2: Theoretical and Experimental Methods:

2.1 - Electronic/Thermal Transport Properties Measurement

Thermoelectric efficiency depends on the relevant transport properties: S, ρ, κ being the Seebeck coefficient, resistivity, and thermal conductivity, respectively. These properties are each measureable to give the thermoelectric figure of merit, zT. Measurements were performed on disc-shaped samples synthesized according to the techniques described in a later section.

2.1a - Electrical Resistivity/Conductivity and Hall Effect

The electrical resistance is a quantity that is simply measured with a multi-meter, but resistivity is an intrinsic material property that does not depend on the amount of material present. The traditional method of measuring resistivity is accomplished with a rectangular prism sample with known cross sectional area, A, as detailed in Figure 2-1a. Here, a known current, I, is passed through the sample through contacts at either end of the prism. The voltage, V, is measured by probes with a known distance between them, L^*, from which the resistance, R, can be estimated from Ohm's law: $R = \frac{V}{I}$. The resistivity, ρ, then is simply calculated using $\rho = \frac{RA^*}{L^*}$. This technique is preferred for samples which are either single crystals or ones with anisotropic properties. For polycrystalline or cubic samples, the Van Der Pauw method is a simpler way to obtain the resistivity(Figure 2-1b). Here, a known current is passed through two leads attached to a disc shaped sample with known thickness, t. The voltage is measured perpendicular to the current flow. In a second step, the current is flowed perpendicular to the first step's current, and the voltage is measured on the remaining two leads. The resistivity can be calculated using the Van der Pauw formula $e^{-\frac{\pi R_1 t}{\rho}} + e^{-\frac{\pi R_2 t}{\rho}} = 1$, where R_1 and R_2 are the measured resistances. In addition to measuring the resistivity for the sample, additional information can be obtained upon performing these measurements under a magnetic field. The Hall voltage can be measured by

applying a magnetic field, *B*, perpendicular to the flowing current, *I*, in both the bar sample or in the Van der Pauw arrangement. The Hall voltage, V_H, can be measured perpendicular to both *I* and *B*, from which the carrier concentration can be estimated: $n_H = -\frac{IB}{teV_H}$. Once the number of carriers is known, the mobility (μ_H) of those carriers can also be expressed from the measured conductivity (inverse of resistivity): $\sigma = n_H e \mu_H$. While the simple measurement of the resistivity is all that is required for estimation of the thermoelectric performance (*zT*), the Hall carrier concentration and mobility provide much needed additional information about the underlying transport and charge carrier scattering mechanisms (also the sign of the Hall coefficient—$R_H = \frac{1}{n_H e}$—indicates the sign of the majority charge carrier).

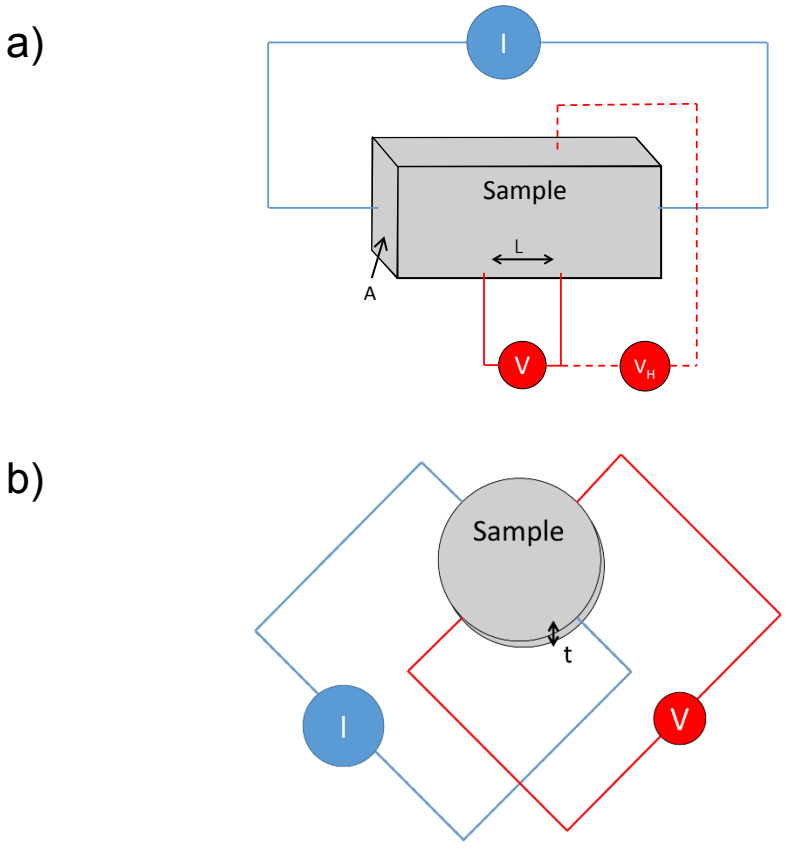

Figure 2-1: Electrical resistivity measurement schematic a) Conventional bar sample, b) disc-shaped sample via the Van Der Pauw method.

In this thesis, all of the measurements are performed on polycrystalline hot-pressed disc-shaped samples (synthesis procedure described in a later section) in the Van der Pauw arrangement in a ±2 T magnetic field using niobium pressure contacts [31]. The temperature is varied from room temperature up to ~500-600°C with the entire setup under high vacuum to avoid sample oxidation.

2.1b - Seebeck Coefficient

The Seebeck coefficient is measured in an instrument built and designed in the Snyder group lab as described in detail by Iwanga et al. [32] Essentially, two thermocouples are constructed by passing two unlike metal wires (chromel–niobium) through thin rods with 4 narrow holes. The wires are threaded through at the end of the ceramic rod (Figure 2-2) to form a single point of contact (which is pushed onto the sample using a spring); this contact allows for both voltage and temperature to be measured at the sample surface. Temperature is measured by measuring the voltage difference between the two thermocouple wires (which are on the same side of the sample) and comparing this voltage to a reference junction at a known temperature. The Seebeck voltage is found by measuring the voltage difference across the sample with two alike wire types, i.e., niobium only. The thermocouples and narrow ceramic rod (both top and bottom) are passed through a larger, heated ceramic block which also makes direct contact to the sample. The heating serves two purposes: first, the cold-finger effect through the thermocouple probe is reduced so that the temperature at the sample surface can be accurately deduced, and second, to maintain good thermal contact with the sample to establish the temperature gradient.

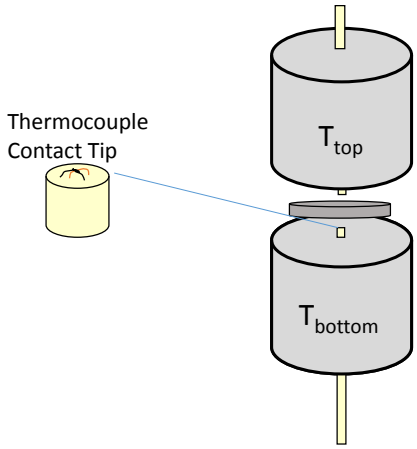

Figure 2-2: Schematic of the uniaxial Seebeck coefficient measurement setup.

During high temperature Seebeck coefficient measurements, rather than simply heating one side to a slightly higher temperature, taking a voltage measurement, and calculating the Seebeck coefficient as the voltage divided by the temperature difference, we perform temperature oscillation sequences. Here, the top and bottom temperatures are made to oscillate giving a range of different temperature differences within $\pm 10\,K$. The resulting voltages and temperature differences are plotted and a linear fit is performed to extract the Seebeck coefficient. We find that this method compensates for any systematic errors and gives accurate and reproducible results. Because the Seebeck coefficient is squared in the final estimate of *zT*, it is critical to reduce error in this measurement (a 10% error in Seebeck propagates to a 20% error in zT). Several "round robin" measurement cycles have been performed to determine what spread of properties measured on different instruments can be observed [33].

2.1c - Thermal Conductivity

Thermal conductivity has, of the three properties in *zT*, been one of the more difficult to accurately measure over the years. In the simplest case, the measurement is performed by passing a known power through a well-insulated sample and measuring the temperature at different points. Unfortunately, careful calibration is required to account for radiative losses, especially at high temperatures. Recently, the standard for thermal measurements in the thermoelectrics

community has changed towards measuring the thermal diffusivity using the commercial Netzsch Laser Flash Apparatus (LFA 457). In this technique, a laser pulse slightly heats the sample surface inside of a furnace (which is heated to the desired measurement temperature). An optical detector carefully measures the time-dependent temperature increase and decrease at the sample surface. A model (Cowan Model with Pulse Correction) is used to correlate this time-dependence directly to the thermal diffusivity, $D = \frac{\kappa}{dC_p}$, where κ is the thermal conductivity, d is the sample density, and C_p is the heat capacity. The sample density is usually either measured directly (by estimating the volume from the sample thickness and diameter, and the mass by weighing with a scale), or it is estimated from the lattice parameter (which can be obtained from x-ray diffraction). All of the samples were coated with a thin layer of graphite to minimize emissivity errors. The heat capacity is sometimes estimated using the Dulong–Petit method (C_p = 3 k_B per atom) (as in the ZrNiSn case), or it is extracted from previous literature in the case of the IV-VI materials [34].

2.2 - Optical Properties Measurement and Analysis

Optical properties measurements have been used extensively in this work to provide information about the electronic states near the band gap. I do this by analyzing the optical absorption edge (as discussed in the introduction). In order to experimentally measure the frequency dependent absorption coefficient, several techniques can be used. In this thesis, I have chosen to focus on Diffuse Reflectance Infrared Fourier Transform Spectroscopy (DRIFTS), which is straightforward to perform and yields consistent results. In DRIFTS, a light source (black body radiator) illuminates a sample by way of an ellipsoidally shaped mirror (See Figure 2-3). The sample, which is usually a finely ground powder, diffusely reflects the light in all directions. The reflected light is collected with the ellipsoidal mirror and refocused onto a detector. Kubelka Munk theory derives a simple relation between the fraction of reflected light (R) and the absorption coefficient (α):

$$F(R) = \frac{\alpha}{\tilde{K}} = \frac{(1-R)^2}{2R} \qquad \text{Equation 2-1}$$

where $\tilde{K}$ is the scattering coefficient (an unknown parameter). Figure 2-3b shows some measurement results from a few relevant thermoelectric materials. I observe the correct ordering of the absorption edges in these materials: Bi_2Te_3 (~0.1 eV), PbSe (~0.27 eV), PbTe (~0.29 eV), and PbS (~0.42 eV), consistent with literature results.

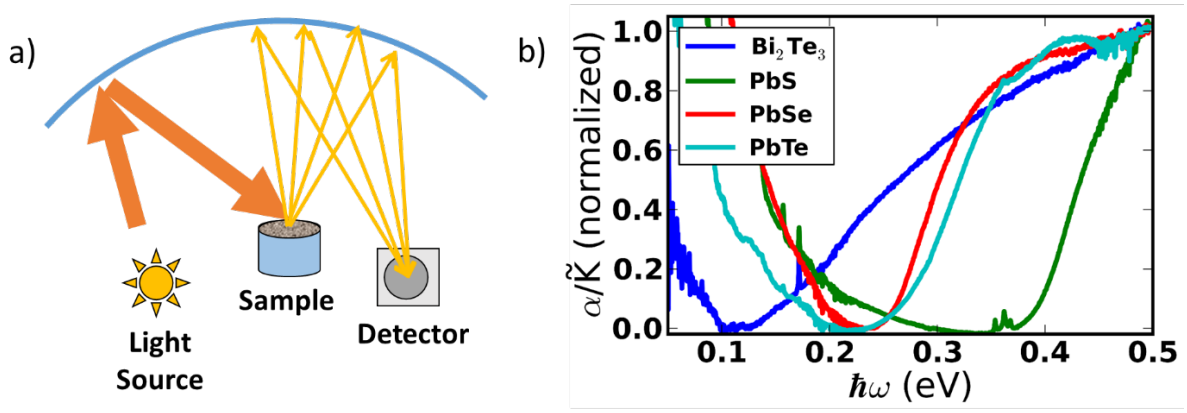

Figure 2-3: a) Schematic of the Diffuse Reflectance technique for measuring spectral absorption. b) Representative DRIFTS results for several relevant thermoelectric materials (at 300 K).

For particle sizes greater than the light wavelengths measured (20 - 2 μm), the scattering coefficient is understood to be approximately independent of frequency [35]. For all measurements in this thesis, I use a Nicolet 6700 FTIR Spectrometer with a deuterated triglycine sulfate (DTGS) detector equipped with a KBr beamsplitter. All samples were referenced to the provided alignment mirror, this was found to give nearly same results as when referenced to KBr powder without the added impurity features from KBr itself. This optical setup gave good spectral intensity for photon energies between ~0.05 eV up to 0.8 eV (with severely deteriorating spectral quality above ~0.6 eV). This range was ideal for studying most thermoelectric materials, which

are usually narrow gap (E_g<0.5 eV) semiconductors. Several other methods for measuring the optical properties are available for materials with gaps in this range.

Many of the previous reports of optical band gap measurements on PbTe have used single crystal samples measured in transmission [27, 36-42]. Transmission experiments have a few disadvantages: first, optically transparent single crystals are often used to avoid internal reflections and light scattering at the grain boundaries, which are generally more difficult to prepare than polycrystalline powder samples. Second, the samples must be polished quite thin since the absorbance scales exponentially with the absorption coefficient and sample thickness through Beer's law, $A = \exp(\alpha t)$, where α is the absorption coefficient and t is the sample thickness. This limits the highest absorption coefficient that can be measured for a given sample thickness. Lastly, in cases where the samples were sufficiently thin (i.e., thin film samples with thicknesses on the order of the light wavelength), oscillations can result in the measured absorbance. These Fabry-Perot fringes are related to interference during internal reflection. While the effect can be mitigated through mathematical models, additional analysis is required.

Diffuse reflectance infrared Fourier transform spectroscopy (DRIFTS) was used exclusively in this work for optical measurements due to its ease of sample preparation and data analysis. Diffuse reflectance can be obtained in a thin sample layer of a ground powder. The measurement requires only a small amount of polycrystalline sample (200 mg or less). Because of the Fourier transform analysis, light at all frequencies can be measured simultaneously, greatly reducing sampling time relative to techniques which vary frequency using a diffraction grating. Relating the diffuse reflectance to sample absorption can be performed using the Kubelka-Munk function (Equation 2-1). Chapter 3 of this thesis shows that DRIFTS is very sensitive to small changes in the energy of direct transitions across the band gap due to progressively higher doping levels. With proper extrapolation the small shifts associated with doping can be shown and understood according to existing optical analysis techniques. Additionally, small, temperature-dependent shifts in the band

structure can be detected using a high temperature stage (as shown in Chapter 4 and Chapter 6). A Praying Mantis attachment (Harrick) was used to collect the DRIFTS spectra. A high/low temperature stage, also from Harrick (CHC), was also used to vary the sample temperature from 120 to 673 K. Measurements were performed under an argon atmosphere after rough pumping and purging the sample chamber several times. Temperature dependent scans were referenced to either KBr standard samples taken at the same temperatures or a room temperature scan of the alignment mirror (although both references gave similar results).

2.2a - Optical Band Gap Extraction

The theory of optical transitions in semiconducting materials is discussed in detail in many references [43-45]. Typically, the method of extraction of the optical band gap depends on the type of transition observed. In the case of direct transitions, electron crystal momentum, *k*, is conserved. As is the case in PbTe, which has its valence band maximum and conduction band minimum at the same points in *k*-space (the *L*-point), direct transitions simply require the incoming photon to impart its energy on the valence-band electron. In this case, the absorption coefficient is proportional to the joint density of states, which in the case of two parabolic bands has the form:

$$\boldsymbol{\alpha\hbar\omega} \propto \left(\hbar\boldsymbol{\omega} - \boldsymbol{E_g}\right)^{\mathbf{1/2}} \qquad \text{Equation 2-2}$$

for $\hbar\omega > E_g$ according to the Tauc method [45, 46]. Other authors have plotted α^2 vs. $\hbar\omega$ for fitting the direct gap[37], but both methods give similar results (within the measurement error ~0.005 eV).

Many semiconducting systems contain indirect band gaps. For example, silicon has an indirect gap from the valence band at the Γ point to the conduction band which lies along the $\Gamma - X$ line [47]. For indirect gaps, i.e., where the initial and final electron momentum is not the same, either emission or absorption of a phonon (a lattice vibration) is required in order to shift *k* to its final value. Generally, even the highest energy phonons have energies on the order of 10-50 meV,

and therefore do not impart much energy in comparison to the photons required for excitation. In the case of indirect absorption the absorption coefficient is known to scale as:

$$\boldsymbol{\alpha\hbar\omega \propto \left(\hbar\omega - E_g\right)^2} \qquad \text{Equation 2-3}$$

following the same Tauc-formula as direct gap, but with a different exponent. Some works suggest $\alpha \propto \left(\hbar\omega - E_g\right)^2$, but as was the case in direct gaps, the results do not change significantly. Nonetheless, because indirect gaps require both a phonon and a photon simultaneously, their transitions often occur with much lower probability (a factor of 10-100x less [48]). However, because the transition frequency inherently depends on the number of valence and conduction band states, indirect transitions from states with significantly larger density of states than direct ones can still have a large absorption magnitude, as we will show in $CoSb_3$ and other systems in Chapter 5.

Optical band gaps in this work were generally obtained using the Tauc method (unless otherwise specified), where $(\alpha\hbar\omega)^n$ and where *n*=2 for direct transitions and *n*=1/2 for indirect. The Tauc function is extrapolated on a plot versus photon energy, $\hbar\omega$, to zero (normalized) absorption; the zero is determined by either normalizing the sample to the minimum absorption coefficient value or by fitting and subtracting the free carrier absorption contribution: $\alpha_{FC} = a(\hbar\omega)^b + c$ (which will be discussed more thoroughly in Chapter 3).

2.3 - Estimating Band Gap from Temperature Dependent Electronic Properties

As mentioned in Chapter 1, there are several experimental methods of measuring the band gap, both using electronic and optical properties.

2.3a - Resistivity

First, the band gap can be estimated from electronic resistivity for an intrinsic semiconductor (where the number of holes and electrons are approximately equal). In the case where the

electron and hole mobilities the same, one can derive that the temperature dependent resistivity should decrease in the intrinsic region as:

$$\boldsymbol{\rho \propto \exp(\frac{E_g}{2k_BT})} \qquad \text{Equation 2-4}$$

where E_g is the band gap, and T is the temperature. The band gap can be extracted from the slope of a plot of log of resistivity as a function of $1/T$. This is a common technique for determining the band gap in semiconductor materials in the absence of other estimates, but the linear region will not be reached if the materials is too heavily doped. In that case, the resistivity will behave as a metal, i.e., increasing resistivity with temperature.

2.3b - Band Gap Estimate from the Maximum Seebeck Coefficient

Alternatively, the peak in the Seebeck coefficient can be used to estimate the band gap of a material. At low temperatures, a sufficiently doped sample will have an increasing Seebeck coefficient with temperature (approximately linear with temperature in the degenerate limit). At sufficiently high temperatures (i.e., when E_g~O(k_BT)), a sufficient population of minority carriers develops which slows the increase in Seebeck coefficient, eventually resulting in a maximum in the thermopower. Goldsmid and Sharp have developed a relationship between the maximum Seebeck coefficient and the band gap [49-51]:

$$\boldsymbol{E_g = 2S_{max}T_{max}} \qquad \text{Equation 2-5}$$

Similar to the temperature-dependent resistivity, this requires similar assumptions about the relative mobility of holes and electrons. This assumption turns out to be quite important for materials such as ZrNiSn [52], which I will explore in detail during this thesis in Chapter 5. I also developed a method for determining how far the band gap will deviate from the Goldsmid-Sharp estimate as a function of the electron-to-hole weighted mobility ratio, A, even for materials with narrow gaps (or moderate gaps at high temperature) [50]. The Goldsmid-Sharp band gap is usually assumed to be, at best, a qualitative estimate (within ~20%). For a more direct

measurement of band gap, optical methods are preferred, although they are not always feasible in doped samples.

2.4 - Band Engineering

Band engineering is a common topic in this thesis which involves optimization of thermoelectric efficiency through modifications in the electronic band structure. This can involve either tuning the Fermi level (E_F) through doping to optimize the thermoelectric properties or alloying the material with another to alter the electronic structure to improve thermoelectric properties (possibly through band convergence).

2.4a - Single Parabolic Band Model – Carrier Concentration Optimization

The most straightforward way to optimize a thermoelectric material is by varying the doping content and charge carrier concentration. Improvements in this context are often explained using the "single parabolic band model" where the material properties are assumed to be described by a free electron-like band with a certain effective mass (some multiple of the mass of a free electron). In terms of the thermoelectric figure of merit, zT, the optimum value can be found to scale with the quality factor:

$$\boldsymbol{B} = \frac{\boldsymbol{2k_B^2\hbar}}{\boldsymbol{3\pi}} \frac{\boldsymbol{N_v C_l}}{\boldsymbol{m_c^* E_{def}^2 \kappa_L}} \qquad \text{Equation 2-6}$$

where k_B is the Boltzmann constant, $\hbar$ is Planck's constant ratioed to 2π, N_v is the valley degeneracy, $C_l = dv_l^2$ (where d is the density and v_l is the longitudinal speed of sound), m_c^* is the inertial effective mass, E_{def} is the deformation potential (which is a measure of the strength of coupling between lattice vibrations and electronic structure), and κ_L is the lattice thermal conductivity.

The single parabolic band model is derived from the Boltzmann transport equation using the relaxation time approximation to obtain the thermoelectric parameters as a function of the reduced chemical potential [24, 53, 54], $\eta = \frac{\xi}{k_B T}$, where ξ is the electronic chemical potential (which reduces to the Fermi level, E_F, at T=0 K). The resulting relations for the thermoelectric transport properties are written below for an arbitrary power law dependence of the scattering time: $\tau(\epsilon) = \tau_0 \epsilon^{\lambda - 1/2}$ [24].

$$\boldsymbol{S(\eta) = \frac{k_B}{e}\left[\frac{(2+\lambda)}{(1+\lambda)}\frac{F_{1+\lambda}(\eta)}{F_\lambda(\eta)} - \eta\right]} \qquad \text{Equation 2-7}$$

$$\boldsymbol{n(\eta) = \frac{1}{2\pi^2}\left(\frac{2m_d^* k_B T}{\hbar^2}\right)^{\frac{3}{2}} F_{1/2}(\eta)} \qquad \text{Equation 2-8}$$

$$\boldsymbol{r_H(\eta) = \frac{3}{2}F_{1/2}(\eta)\frac{\left(\frac{1}{2}+2\lambda\right)F_{2\lambda-1/2}(\eta)}{(1+\lambda)^2 F_\lambda^2(\eta)}} \qquad \text{Equation 2-9}$$

where λ determines the scattering exponent, n is the charge carrier concentration, m_d^* is the density of states effective mass, r_H is the Hall coefficient, which determines the relationship between the measured $n_H = \frac{1}{R_H e}$ and the chemical carrier concentration ($\frac{n}{n_H} = r_H$), and $\epsilon = \frac{E}{k_B T}$. $F_j(\eta) = \int_0^\infty \frac{\epsilon^j d\epsilon}{1+\exp(\epsilon-\eta)}$, which is defined as the j^{th} order Fermi integral. While there are analytical expressions for the transport integrals in either the non-degenerate (semiconducting/insulating $\eta \ll 0$) or the degenerate (heavily doped semiconducting/metallic $\eta \gg 0$) limits, the best thermoelectric materials tend to have Fermi levels somewhere in the intermediate region (η near the band edge), requiring a full, numerical solution to the Fermi integrals (Python, Matlab, Mathematica, Excel/VBA). For most thermoelectric materials at or above room temperature, acoustic phonon scattering is the dominant scattering mechanism, and it usually works well to describe transport in thermoelectric materials, requiring: $\lambda = 0$ and $\tau_0 = \frac{\pi\hbar^4 C_l}{\sqrt{2}E_{def}^2 (m_b * k_B T)^{3/2}}$. Here,

m_b^* is the single valley effective mass (neglecting the effects of valley degeneracy). For systems where acoustic phonon scattering dominates, mobility decreases with temperature roughly as $T^{3/2}$ (although some variation can exist if the effective mass is also temperature dependent). The real usefulness of Equation 2-7 through Equation 2-9 is that they relate experimentally measured parameters (Seebeck coefficient and Hall carrier concentration) back to the electronic band structure. The effectivez mass (which when estimated from the SPB Seebeck and carrier concentration, we will call m_S^*) is directly related to the band curvature and valley degeneracy ($m_d^* = N_v^{2/3} m_b^*$). In order to obtain m_S^*, first, the measured Seebeck coefficient will be used to estimate the reduced chemical potential (η) using Equation 2-7. η can be substituted into the measured $n_H = \frac{n}{r_H}$, the ratio of *n* (Equation 2-8) to r_H (Equation 2-9), to solve for the experimental effective mass (m_S^*). m_S^* is believed to represent the density of states m_d^*, rather than the conductivity mass defined previously or the single band mass m_b^*.

However, the effective mass is not the only useful parameter obtained in the single parabolic band model. Because Hall-effect measurements also yield the charge carrier mobility, $\mu_H = \mu_0 \frac{\left(\frac{1}{2}+2\lambda\right)F_{2\lambda-\frac{1}{2}}(\eta)}{(1+\lambda)F_\lambda(\eta)}$, it is straightforward to determine the parameter which scales the mobility, $\mu_0 = \frac{e\tau_0}{m_c^*}$, if the value has been measured experimentally. In fact, the band parameters in τ_0 (and the parameters that make it up as indicated in the previous paragraph) can also be determined if we assume that $m_c^* = m_b^* = m_d^*$, essentially requiring a single spherical Fermi surface. The thermoelectric quality factor, *B* (Equation 2-6), can be expressed in terms of μ_0:

$$\boldsymbol{B = \frac{\mu_0 m_S^{*3/2}}{\kappa_L}}$$ Equation 2-10

In addition, the lattice thermal conductivity can be estimated using the Wiedemann-Franz law, $\kappa_L = \kappa - \kappa_e = \kappa - L\sigma T$, where $\kappa_e = L\sigma T$ is the electronic thermal conductivity. The expression for the Lorenz number, *L* is given by:

$$\boldsymbol{L = \frac{k^2}{e^2}\frac{(1+\lambda)(3+\lambda)F_\lambda(\eta)F_{\lambda+2}(\eta) - (2+\lambda)^2F_{\lambda+1}^2(\eta)}{(1+\lambda)^2F_\lambda^2(\eta)}}$$ Equation 2-11

By computing m_S^*, μ_0, and κ_L from experimental data, we can make a plot of the carrier concentration dependent thermoelectric properties, as shown in Figure 1-2. The power of this simple method is that this plot can be generated after making and measuring the *zT* for a single sample. We can immediately determine the value of the maximum *zT*, and whether the charge carrier concentration needs to increase or decrease to yield the optimum *zT*. Usually, a series of samples is made with different doping concentrations to reduce the uncertainty of the m_S^*, μ_0, and κ_L values.

2.4b - Valley Degeneracy and Band Anisotropy

Higher levels of complexity can be added to the single parabolic band transport model. To begin with, perhaps the most profound in terms of thermoelectric enhancement are the valley degeneracy (N_v) and band anisotropy (*K*). Each of these show up during several chapters of this thesis. The valley degeneracy, N_v, is defined as the number of distinct charge carrier pockets (of the same sign) which exist at the Fermi level. The origin of these degeneracies can be broken down into two parts: $N_v = N_{v,symmetry}N_{v,band}$, where $N_{v,symmetry}$ is related to the degeneracy of a given point in the Brillouin zone due to that point's symmetry and $N_{v,band}$ which is the number of individual bands that are converged at that energy. Valley degeneracy manifests itself by increasing the density of states effective mass, $m_d^* = N_v^{2/3}m_b^*$, relative to the single valley effective

mass (m_b^*). This is beneficial for the thermoelectric properties because each individual pocket conducts in parallel while the overall Fermi level does not rise too quickly (allowing the material to maintain a high Seebeck coefficient). In order to maximize N_v, a highly symmetric Brillouin zone (usually found in high symmetry materials) with band extrema that exist at low symmetry points lead to the highest degeneracy. For PbTe and other IV-VI materials, the primary valence band exists at the L-point with $N_{v,symmetry}$=4, and a $N_{v,band}$=1, and a secondary band exists along the Σ line with a high degeneracy of $N_{v,symmetry}$=12, and a $N_{v,band}$=1.

The common definition for the effective mass is $m^* = \hbar^2 \left(\frac{d^2E}{dk^2}\right)^{-1}$, which is the inverse of the curvature of the band in energy vs. *k*-space (light bands have high curvature, heavy bands have shallow). In the simplest case, this Fermi surface will have the same curvature along all directions in *k*-space, producing a single, spherically shaped pocket. However, for many common materials this is not the case (Si/Ge [55, 56], III-V [57], and the lead chalcogenides [58-60]). In general, the effective mass can be different along all three directions. For example, when describing the density of states in that band, the geometric average along these directions is most appropriate: $m_d^* = N_v^{2/3} m_b^* = N_v^{2/3} (m_1^* m_2^* m_3^*)^{1/3}$, where N_v is the valley degeneracy, m_b^* is the single valley effective mass, and $m_{1,2,3}^*$ are the effective masses along the different directions. While the density of states effective mass is the appropriate scaling parameter for the carrier concentration, the electrical conductivity and mobility are governed by the harmonic average over the different directions, yielding the conductivity (or inertial) effective mas: $m_c^* = \frac{3}{\frac{1}{m_1^*}+\frac{1}{m_2^*}+\frac{1}{m_3^*}}$, which weights the lighter (higher conductivity) directions more. Most often experimentally, Fermi surfaces are believed to be ellipsoidal, implying $m_1^* = m_2^* = m_\perp^*$ and $m_3^* = m_\parallel$. Often, the anisotropy is described by the parameter $K = \frac{m_\perp^*}{m_\parallel^*}$. While it is possible to obtain information about the band anisotropy directly from experiments (Faraday rotation [55, 56], Shubnikov De Haas [61]), for new materials these experiments have usually not been performed; therefore *K* is assumed to be 1.

2.4c - Multiple Band Effects

As is the case in p-type PbTe, many good thermoelectric materials exhibit multiple band effects. While semiconductors are inherently multi-band systems (one valence, one conduction band), good thermoelectric materials are sufficiently doped, meaning that their Fermi levels are far enough from the minority carrier band to not have detrimental effects to the majority carrier properties. In systems such as PbTe, where a secondary valence band exists about 0.12 eV below the primary, the effects are almost always beneficial to the thermoelectric properties. This can be understood by considering the quality factor, B (Equation 2-6), which is proportional to the valley degeneracy. Any electron (or hole for p-type material) population in an additional band which contributes to the electronic transport properties (i.e., the band's energy is within ~4 $k_B T$ of the chemical potential) can be regarded as an increase in the effective valley degeneracy (a topic that will be discussed in detail in Chapter 7). This increase ultimately results in a better zT than could have been obtained by either band separately; however, the details depend significantly upon the energy offset (ΔE) between the bands. This thesis will focus, in a large part, on the details of these multiple band effects and their characterization and potential enhancement to zT in both an experimentally measureable and theoretical sense.

In order to compute multi-band effects, conductivity weighted averages over the properties of the individual bands (the i^{th} band) are used, as suggested by Putley [62]:

$$\boldsymbol{\sigma} = \sum_{\boldsymbol{i}} \boldsymbol{\sigma_i} \quad \text{Equation 2-12}$$

$$\boldsymbol{S} = \frac{\sum_{\boldsymbol{i}} \boldsymbol{S_i \sigma_i}}{\sum_{\boldsymbol{i}} \boldsymbol{\sigma_i}} \quad \text{Equation 2-13}$$

$$\boldsymbol{R_H} = \frac{\sum_{\boldsymbol{i}} \boldsymbol{\sigma_i^2 R_{H_i}}}{\left(\sum_{\boldsymbol{i}} \boldsymbol{\sigma_i}\right)^2} \quad \text{Equation 2-14}$$

$$\boldsymbol{\kappa} = \boldsymbol{\kappa_L} + \sum_{\boldsymbol{i}} \boldsymbol{L_i \sigma_i T} + \boldsymbol{T}\left(\sum_{\boldsymbol{i}} \boldsymbol{\sigma_i S_i^2} - \boldsymbol{S^2 \sigma}\right) \quad \text{Equation 2-15}$$

where $R_{H,i}$ is the Hall coefficient for the i^{th} band, defined as $R_{H,i} = \frac{1}{n_{H,i}e} = \frac{r_{H,i}}{n_i e}$ (where r_H and n were defined in Equation 2-8 and Equation 2-9). Interestingly, the thermal conductivity shows a non-trivial effect: $\kappa = \kappa_L + \kappa_{e,Lorenz} + \kappa_{bipolar}$. Essentially, the Wiedemann-Franz law accounts for only part of the electronic thermal conductivity in the region where multiple bands exist. The bipolar term is a result of a difference in the total power factor and the power factors of each individual band. In the region where two charge carriers exist with opposite signs (valence and conduction band), the bipolar thermal conductivity is observed rather strongly and is quite important in many thermoelectric materials. In fact, the bipolar effect at high temperature is readily observed in the thermal conductivity (Figure 1-4b) and is one physical origin of the maximum in *zT*. The Seebeck coefficient also is decreased in this bipolar region (Figure 1-4a).

Additionally, the charge neutrality equation:

$$\boldsymbol{N_D} + \sum_{\boldsymbol{i}} \boldsymbol{p_i} = \boldsymbol{N_A} + \sum_{\boldsymbol{i}} \boldsymbol{n_i} \quad \text{Equation 2-16}$$

can be solved with a known number of donors (N_D) and/or acceptors (N_A) (or difference between their concentrations) for the chemical potential dependent electron and hole concentrations (which is only be a function of η given $m_{d,i}^*$ and ΔE are specified for each of the *i* bands at a given T). The charge neutrality equation is useful for determining temperature-dependent thermoelectric properties (assuming N_D-N_A is constant), and it is used in several chapters of this thesis.

It should be noted that the reduced chemical potential for the *i*th band should be defined relative to the first band in order to reduce the overall number of variables (given that the offset between the bands, ΔE, is known). This can be defined as $\eta_i = s_i\eta_1 - \Delta E_{i-1}$, where s_i is the sign of the band (which should be specified relative to that of band 1), ΔE_{i-1} is the band offset between the *i*th and first bands, and η_i represents the reduced chemical potential for that band (which should be substituted into the Fermi integral equations specified previously with the sign of the Seebeck coefficient reflecting the sign of the band, s_i).

2.4d - Band Non-Parabolicity

In this thesis, non-parabolic bands will also be used to describe the thermoelectric transport properties. The two-band Kane model (which Kane originally developed for InSb [63]) involves interacting valence and conduction bands through the $k \cdot p$ method. This model's application to describing electronic transport properties is described in great detail by Zawadski [64] and Ravich [58]. While Zawadski takes a more general approach which includes examples across many material systems and considers a wide range of properties, Ravich's more simple approach is geared towards thermoelectric lead chalcogenides. The equations for the transport properties are outlined in detail in previous work by Wang et al. and will not be repeated here [65], but the relevant Fermi integral is generalized to:

$$ {}^{n}F_{l}^{m} = \int_{0}^{\infty} \left(-\frac{df}{d\epsilon}\right) \epsilon^{n} \left(\epsilon + \beta\epsilon^{2}\right)^{m} \left[(1 + 2\beta\epsilon)^{2} + 2\right]^{l/2} d\epsilon \qquad \text{Equation 2-17} $$

The degree of non-parabolicity is related to the band gap using the parameter $\beta = \frac{k_B T}{E_g}$; therefore materials with small gaps will exhibit large non-parabolicity. In fact, the band edge effective mass can be shown to scale as, $m_0^* = \frac{\hbar^2 E_g}{2P^2}$, where *P* is the interaction matrix element between electrons and holes. In this thesis, I will apply non-parabolic models for the lead and tin chalcogenides and $CoSb_3$. In Chapter 6, I discuss the effect of non-parabolicity on the effective mass, which is obtained through the Seebeck coefficient (m_S^*) by deriving the Mott relation for Kane-type bands.

The generalized Fermi integrals for non-parabolic bands can be used in place of parabolic ones (in fact, if we take $\beta = 0$ the result reduces to the parabolic expression) when computing the properties for either a single or a multi-band transport model.

2.5 - Ab-Initio Calculations

Density functional theory (DFT) calculations are commonplace in materials and chemistry research. In the context of thermoelectric materials, they give a detailed description of the materials' electronic structure, which is critically important to characterizing experimentally measured results. This thesis uses these calculations throughout to guide the research and provide a framework for which to understand the results. Because of the range of methods used by our collaborators, specific details of each calculation will be given within each chapter on the *ab-initio* results obtained.

2.6 - Sample Preparation

Thermoelectric samples were prepared using conventional solid-state chemistry techniques. The IV-VI materials (PbTe, PbSe, SnTe, and their alloys) were prepared by first weighing stoichiometric quantities of the elements, loading them into a quartz ampule, sealing under vacuum, and melting in a tube furnace for approximately 1 day at 1000 – 1100°C. The melted samples were quenched in water followed by annealing for ~ 3 days at 600°C to homogenize the sample.

$CoSb_3$ samples were synthesized in a similar manner to the IV-VI materials where the elements were melted (1080°C) and annealed (for 7 days at 600°C) within boron nitride crucibles that were sealed within quartz ampules.

Half-Heusler (ZrNiSn) samples were prepared via arc-melting due to the high melting point of Zr. The arc-melting of the elements occurred in an Ar atmosphere within a water-cooled copper crucible. To ensure compositional homogeneity, samples were flipped and remelted five times.

The as-cast samples were annealed in evacuated quartz tubes at 1220 K for 7 d, followed by quenching in ice water to ensure the crystalline order.

For each of the materials, the samples were quenched after annealing and the ingots were recovered and ground into a fine powder (in the glove box). Samples were prepared by loading this powder into a graphite dye (1/2” outer diameter) which was used for induction hot-pressing [66]. The resulting samples were high quality (>95% theoretical density) ½” discs which were polished and prepared for the electrical, thermoelectric, and thermal measurements required to estimate zT. X-ray diffraction was performed to ensure that the expected crystal structure was obtained and to discover any possible secondary phases (detection limit of ~1%). Additional details regarding the synthesis, as needed, will be included at the end of each section.